Original Article

Received: 2021-11-08
Accepted: 2021-12-02

BCCR
2021, No 4, Vol 13 :305-319
www.bccrjournal.com

Comprehensive Study of Lung Cancer Proton Therapy with Injection of GNPs

Reza Khoramdel, Seyedeh Nasrin Hosseini Motlagh*, Zohreh Parang

1

Department of Physics, Shiraz Branch, Islamic Azad University, Shiraz, Iran

Email:nasrinhosseinimotlagh@gmail.com

ABSTRACT

The application of radiation therapy (RT) in lung cancer has shown some exciting and sometimes disappointing advances in recent years. Protons compared with photons interact differently with human tissues, and can be used to improve patient care for suffering from lung cancer. A new strategy is the simultaneous injection of nanoparticles with proton radiation into the tumor which has been given over a decade to improve conventional RT. In this work, proton beam therapy (PBT) with gold nanoparticles (GNPs) is used as a part of a combination program to treat advanced localized lung cancers. This paper aims to develop the complex Geant4 model on the human lung and predict the distribution of absorbed dose in lung tumors during proton therapy without and with a high-Z injection of GNPs. Thus, the absorbed dose distribution in lung tumors for four modes such as (i) Bethe-Bloch's relativistic quantum theory, (ii) GEANT4/GATE7 simulation model, (iii) Hartree-Fock-Roothaan(HFR) wave functions, and the (vi) Bortfeld theoretical model without and with the injection of GNPs in predicted lung phantom are compared.

Keywords: Lung, Nanoparticles, Proton, Relativistic, Simulation

INTRODUCTION:

One of the leading cancers around the world is lung cancer. Lung cancer is divided into two main branches depending on the type of cancer cells: Small and non-small cell lung cancer. Due to the difficulty of treating lung cancer, this cancer can be considered the most common type of cancer that can lead to death, both in men and women. It is important to know which type of lung cancer is affected, because small cell cancers have the best response to chemotherapy, while other types, often referred to as large lung cancers, are better treated with surgery or radiotherapy [1]. Since the 1960s, RT using photon radiation therapy (XRT) has been one of the most common methods for treating lung cancer [2]. Despite years of research, the result is that treating patients with lung cancer is generally weak due to their cancer's tendency to metastasize using XRT. Therefore, studying the more precise treatment of lung cancer is essential. An effective way to improve the outcome of cancer treatment is RT optimization. Historically, the patient's therapeutic outcome is improved if newer radiation patterns are invented. For the first time, the radiotherapy procedure was performed using radioisotopes that were placed directly inside the tumor. This method causes problems in the treatment of lung cancer from the moment the source is placed in the lung tumor, and as a result, the lung is damaged. Subsequently, low-energy X-rays were created that injected KV X-rays into lung cancer tissue. Unfortunately, these rays penetrate slightly into the tissues and deliver the highest dose to the skin, so only a small portion of the dose is deposited inside the tumor. Then, the cobalt isotope with an atomic number of 60 was used and γ- rays with two different energies of 1.17 and 1.33 million volts were generated and passed through the skin and resulting in deeper penetration of the dose.

Then linear accelerators were developed that produced X-rays with MV energy. These X-rays penetrated more, but still, the maximum dose was deposited between 1.5 and 3.5 cm. Gradually the absorption rate decreased during penetration so that the radiation without stopping was transmitted directly out of the body. The distribution of photon beams in the human body is due to their unique characteristics. Photons are massless and have no electric charge. At first, accelerated protons enter the human body with high momentum, which can penetrate to a certain depth depending on the initial kinetic energy given to them by the accelerator (such as a synchrotron or cyclotron). As the beam of protons travels to this depth, relatively little energy is transferred to the tissue, and the speed of the protons gradually decreases, and then the energy is transferred to the adjacent tissues. The deposited energy per unit length of the path is inversely proportional to the proton's square velocity. In a short period time, before all the proton energy is wasted, the rate of energy loss is maximized. When the kinetic energy of a proton is completely deposited in the tissue, the proton inside the body can be stopped. Energetic protons collide with the electrons of atoms in neighboring tissues, causing them to ionize and eventually damaging the radiation. The area in the body where the most energy is wasted and the final cessation of protons occurs is narrow and depends on the initial energy of the proton beam. The peak that represents the maximum dose due to charged particles is called the "Bragg peak". Beyond this point, as the protons stop, no radiation energy affects the surrounding tissues. Here we are only talking about mono-energetic proton beams. But the peak of the monoenergetic proton beam is very narrow therefore to produce a useful clinical proton beam for the complete coverage of the tumor it is required that the high-dose area is spread which is known as the "spread–out Bragg peak". Clinical data are necessary to prove the success of the patient's delivered dose to improve the patient. The newer proton therapy uses pencil beam scanning instead of passive scattering and uniform scanning pencil beams are very narrow proton beams that are driven by magnetic fields and move forward and backward in a chess pattern inside the tumor volume.

Currently, the introduction of nanoparticles (NPs) as an effective key to improving tumor targeting through the effects of radiation is under investigation. When the tumor containing the NPs is exposed under the beam of

the proton beam, the antibodies or peptides forming the tumor cells are affected. Therefore, a combination of radiotherapy with nano-medicine opens up a new range of therapies. Hainfeld et al, 2008 showed that a core of GNPs with a 1.9 nm diameter, increases mice's lifetime exposure to X-rays of 160 KV [3]. GNPs are already well-known. Other advanced heavy NPs have been made, such as hafnium [4] and gadolinium [5], which have recently been sent to clinics. The role of high- Z NPs has been investigated by Kim et al. To improve proton irradiation performance [6].

They injected small NPs (diameter of 2-15 nm) from Au or Fe into mice tumors that were simultaneously exposed to fast protons with energies of 45 MeV and observed the enhancement of absorbed dose and, consequently, the killing of cancer cells. The efficiency of GNPs has been confirmed by Polf et al in increasing the effects of proton radiation in the laboratory [7]. The group observed a significant increase in the mortality of prostate tumor cells with 160MeV protons when loaded with GNPs. At present, molecular-scale experiments with Pt and Gd NPs have been activated by 150 MeV protons [8]. These NPs are compatible with the body and can be used for treatment [9-11].

We will optimize the conditions relative to the state where nanoparticles are not used. For this purpose, section 2 introduces the characteristics of the suggested phantom used in this study. In section 3, absorbed dose as an important parameter in this work is represented. In section 4, Bethe-Bloch theory is introduced in a completely relativistic state. In section 5, nuclear and electronic stopping power which is a key issue in proton therapy is described. In section 6, HFR atomic wave functions are presented. In section 7 Bragg-Kleemaans law is given. In section 8, Physical parameters in proton therapy are described. In section 9, the Bortfeld model is presented and finally, the conclusions are identified.

2-Proposed lung phantom:

The phantom of the lung tissue is designed to accurately represent the shape and size of the human lung. The dimensions of the lung phantom are: height = 23cm, width = 28 cm, and depth = 13.7cm (see Figure 1). The Geant4 toolkit, version 9.2.02, was chosen as the simulation engine. The water phantom with homogeneous geometry and dimensions 30 × 30 × 40 cm3 was used to simulate Geant4. Dimension x (the beam penetration axis) is determined as the maximum range for proton therapy. The matrix with a size of 1 × 1 × 1 mm3 is set to achieve the results of the data. The entire space, except for the phantom, is filled with air. At a depth of 10 cm inside the suggested phantom, a cubic tumor is placed in a size of 2 cm. Adipose and skin tissue are defined in thicknesses of 0.3 cm and 0.2 cm, respectively.

The phantom material in this geometry is taken from the NIST. This data provides a detailed combination of materials based on the ICRU. Physical models include electromagnetic and nuclear processes. Electromagnetics physics mainly provides the ionization and multiple scattering of each particle based on Lewis's theory for the proton. This theory calculates the spatial distribution as the angular distribution after a stage [12]. Low energy processes up to 250 eV related to photons and electrons such as hadrons and ions can be performed through various models. From electromagnetic physics model based on ICRU49 is used for simulation [13].

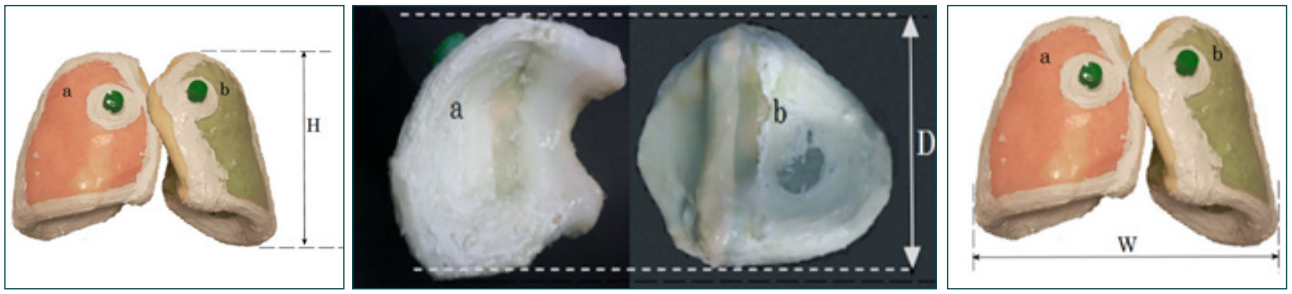

Figure.1. The dimensions of the anatomical lung phantoms a) the right lung b) the left lung. (Hight:H=23cm, Width:W=28cm and Depth:D=13.7 cm)

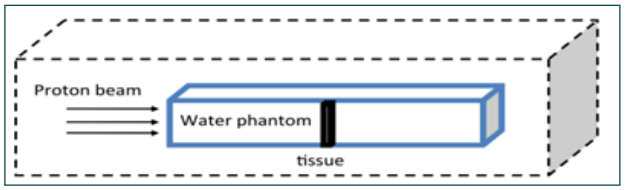

Figure.2. A plan for the selected phantom used in this study.

Nuclear interaction physics is used to study the elastic and inelastic collision between protons and materials. Elastic scattering supports the low energy transfer of proton beams, while inelastic scattering contributes to the nucleon-nucleon interaction in the direction of the proton beam. The G4Pre compound model is used for simulation in nuclear physics. This model is suitable for explaining the interaction in the proton beam energy range and is a good estimation for the production of secondary and neutron particles because it allows the expansion of the low energy range of the hadron kinetic model to the inelastic collision of the nucleus-nucleon. For this simulation, the proton beam is used in the energy range $3 \leq E\,(MeV) \leq 250$ MeV, with Gaussian distribution $\sigma(E)$ in the water phantom. The source of the proton is a pencil beam scanning type that is located 10 cm far from the top level of the phantom. The proton source is in the direction of the beam axis (x-axis) and 5×106 particles have been simulated in our calculations. All particles are examined as if their range exceeds the specified threshold of 0.01 mm to be detected. The location of Bragg's peak is the highest point on the dose curve. Range (in g/cm2) is known as the distance between the beam input surface and 80% of the dose endpoint, which is in grams per square centimeter.

3-Absorbed dose:

TAbsorbed dose is defined as the deposited energy per unit mass of the matter and is given by:

$$D[GY]=(E_{dep}\ [eV]\times 1.60217646\times 10^{19}\ [J/eV])/(\rho[kg/cm^3]/V[cm^3]) \quad (1)$$

where E_dep is deposited energy, ρ and V are mass density and volume of absorbing matter, respectively. D is a physical quantity and does not reflect the biological effects of radiation. However, the determination of D is the first point in examining the environmental effects of radiation, both for random effects and for definite effects. Monte Carlo (MC) simulation is recognized as a method required for research on nuclear medicine, radiology and RT. E_{dep} and D have attracted special interest in RT programs [14] and imaging programs involving ionizing radiation [15]. In RT, good treatment planning requires accurate determination of the absorbed dose distribution in the target organ and tissue. Many MC simulators for imaging [16-18] or dosimetry [19-24], have been developed. Currently, GATE [25,26] is the only MC simulator software suitable for imaging, RT and dosimetry in an environment. GATE originates from GEANT4 software that simulates particles and materials. GATE offers high-level features to simplify the GEANT4-based simulation design. GATE can be improved by OpenGate, and users can access source code [27-28], and introduce new features. GATE can essentially be effective for a variety of simulations, including simulations that study the absorbed dose. Although GATE is well accepted and useful for a variety of PET and SPECT studies, there are currently few users who use this code in dosimetry. GATE uses a mechanism which is known as the Actor Dose, which records the absorbed dose in a specific volume in a three-dimensional matrix. From the point of view of macro-scale GATE, Actor Dose should be linked to the volume being studied. The user can specify the matrix size in such a way that the location of the matrix defined in the volume control system is consistent. Note that if the user defines the size of the matrix more than the desired volume, the deposited absorbed dose will be outside this volume and therefore will not be stored within the network. The Actor evaluates E_dep in MeV and D, in Gy.

$$D_k=\sum_i^N d_{k,j),}S_k=100\times S_k/D_k \quad (2)$$

Eq. (2) defines the statistical uncertainty ε_k in kth pixel, for N value, which represents the initial number of events. d_k, is the deposited energy in kth pixel. D can be calculated as the dose in water, which is commonly

used in RT [29-31]. This conversion is done by taking into account the relative stopping power (SP) and transmitted energy through nuclear interactions in a given environment.

Along the particle tracking path, the deposited energy inside the matrix is added for each step that occurs in the corresponding volume. Two endpoints of a stage, are before and after points. For a particle being tracked, a location is considered randomly, and the corresponding values are stored in the matrix of that location. The user must be sure that the step length is not too large due to the matrix selection. The output can be stored in an MHD image format [32]. Users can manually assign a substance to any Hounsfield units range. Two mixtures with the same composition of elements, but with different densities are examined as two separate materials. Each needs to determine the cross-sectional area and SP, which can be problematic if too much material is used [33]. The number of required materials can be adjusted by the tolerance parameter in GATE [34]. Table 1 lists the different compositions of the elements and the mass densities of some tissues in the human body.

4-Bethe- Bloch Model:

We do not discuss the Bethe-Bloch model in detail, but just examine the aspects of this model for proton therapy. The average dissipated energy rate per unit length of a relatively relativistic charged particle is represented in detail by the Bethe-Bloch equation [35]:

$$dE/dx=(nz^2 e^4)/(4\pi\varepsilon_0^2 m_e v^2)[\{\ln((2m_e v^2)/I)+\Delta L_{shell}\} L_{Bar-kas}+\Delta_{LS}-\ln(1-v^2/c^2)-v^2/c^2-\delta/2+2\ln\gamma-1-1/\gamma^2]\rho \quad (3)$$

The symbols used in this equation are shown in Table 2, respectively. In a low-energy region (less than 10 MeV), when the particle velocity is equal to one of the target electrons (≈0.0073c), ion neutralization due to electron capture plays a crucial role in the stop process, and z must be converted to Z_{eff}, which a semi-experimental relation: $Z_{eff}=z(1-\exp(125z\beta-2/3))$ in which has been extracted from Barks experimental data. In Figs.3a , 3b, 3c, 3d, 3e, 3f, 3g, and 3h, using Maple programming, we plotted the three-dimensional variations of different parameters such as $\beta = v / c$, Barkas correction, shell correction, Lindhard-Sorensen correction [36], density effect, effective atomic number, the total SP and absorbed dose in terms of proton energy beam in the range of $1\leq E(MeV)\leq 250$ and penetration depth in the lung tumor in the range of $1\leq x(cm)\leq 30$ without the injection of GNPs. As shown in the diagrams, each parameter plays a specific role in the determination of SP and absorbed dose, and they are a function of proton penetration depth in the tissue and the proton energy.

5-Nuclear and electronic stopping power:

An energetic ion that penetrates the material loses its energy mainly through two processes that are independent of each other. These two processes are the loss of nuclear

Table 1. Different compositions of elements and mass densities of some tissues in the human body.

Tissues	ρ(g/cm³)	H	C	N	O	Na	P	S	Cl	K	Au
Skin	1.09	10.0	20.4	4.2	64.5	0.2	0.1	0.2	0.3	0.1	-
Soft Tissue	1.03	10.5	25.6	2.7	60.2	0.1	0.2	0.3	0.2	0.2	-
Lung	0.29	10.30	10.50	3.10	74.90	0.20	0.20	0.30	0.30	0.20	-
Tumor	1.040	9.40	21.20	5.60	61.50	0.25	0.51	0.64	0.39	0.51	-
10mgAu/ml	1.05	10.6	14.4	2.2	70.5	0.2	0.4	0.2	0.3	0.3	1.0
25mgAu/ml	1.07	10.4	14.2	2.1	69.5	0.2	0.4	0.2	0.3	0.3	2.3
50mgAu/ml	1.09	10.2	13.8	2.1	67.9	0.2	0.4	0.2	0.3	0.3	4.6
75mgAu/ml	1.12	10.0	13.5	2.1	66.4	0.2	0.4	0.2	0.3	0.3	6.7

Table 2. List of parameters in the Bethe-Bloch equation

Symbol	parameter	Symbol	parameter
n	number density	ε_0	Permittivity constant
e	electron charge	ρ	Material density
m_e	Electron mass	$-\delta/2=-\ln(\beta\gamma)+\ln(1/(\hbar\omega_p))+1/2$	correction of density effect due to dissipated ionization energy
I	The average ionization energy of the target material	$\beta=v/c$	The velocity of proton/ velocity of light
Z	The atomic number of the absorber	$\gamma=1/\sqrt{(1-\beta^2)}$	Lorantz factor
ħ	reduced Planck constant	$L_{Baraks}=1+2z/\sqrt{Z}[F(V)]$ where $F(V)=0.0019\exp(-2\ln(V/10))$	Barkas correction, which indicates polarization effect inside the target environment, resulting from a low-energy collision between the projectile and electrons.
ω_p	plasma frequency of the medium	$\Delta L_{Shell}=-C/Z$ Where $C=(4.22377\times10^{-7}\beta^{-2}\gamma^{-2}+3.04043\times10^{-8}\beta^{-4}\gamma^{-4}-3.8106\times10^{-10}\beta^{-6}\gamma^{-6})I^2+(3.858019\times10^{-9}\beta^{-2}\gamma^{-2}-1.667989\times10^{-10}\beta^{-4}\gamma^{-4}+1.5795510^{-12}\beta^{-6}\gamma^{-6})I^3)$ (which is considered valid for $\beta\gamma\beta\gamma>0.13$).	Shell corrections occur when projectile the velocity is comparable to the electron velocity in target atoms.
$V=\beta\gamma/(\alpha\sqrt{z})$	reduced momentum	$\Delta_{LS}=\sum_{-}[\ k/\eta^2\ (k-1)/(2k-1)\sin^2(\delta_k-\delta_{(k-1)})+k/\eta^2(k+1)/(2k+1)\sin^2(\delta_{(-k)}-\delta_{(-k-1)})+k/(4k^2-1)\ 1/(\gamma^2k^2+\eta^2)-1/k]+\beta^2/2$	Lindhard-Sorensen correction recovers the Bloch correction in the low-energy range, whereas also incorporating Mott scattering in a relativistically correct manner
$\eta=\alpha z/\beta$	dimensionless parameter	$\alpha=e^2/(4\pi\varepsilon_0\hbar c)$	fine structure constant
δ_k	relativistic Coulomb phase shift	k	angular momentum quantum number parameterization covering spin

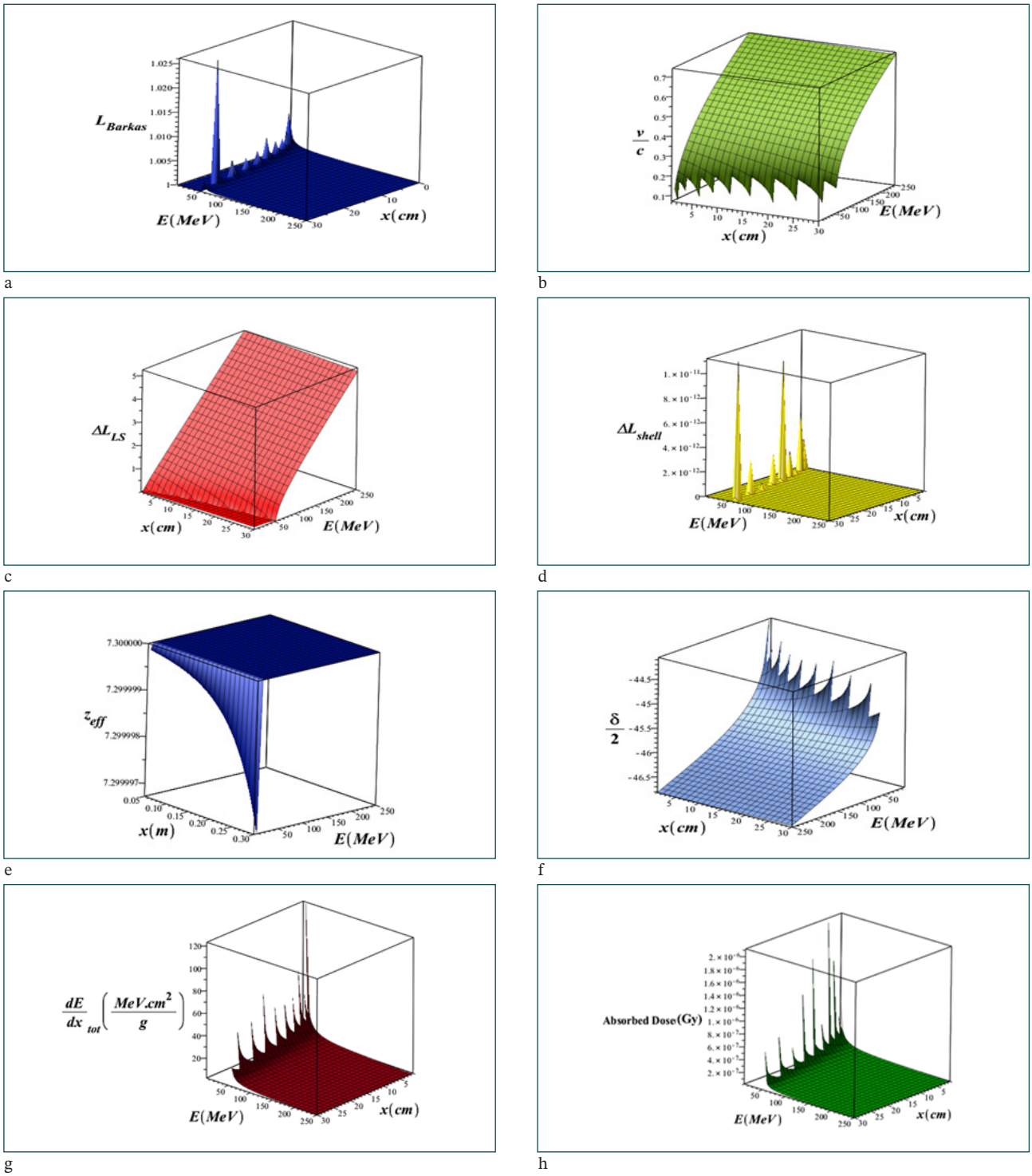

Figure.3. 3D variations of $\beta = v / c$, Barkas correction, shell correction, Lindhard-Sorensen correction, density effect, effective atomic number, total stopping power and, absorbed dose, versus proton beam energy for $1 \leq E\ (MeV) \leq 250$ and penetration depth in the lung tissue in the range $1 \leq x\ (cm) \leq 30$ without the injection of GNPs (using equ. 3)

energy and the loss of electron energy. Thus, the stopping power can be divided into two parts: i) nuclear and ii) electronic stopping power. Nuclear stopping power is calculated by integrating all of the impact parameters:

$$dE/dx_{nuc}=2\pi\int_0^{bmax}T(E,\alpha)bdb \quad (4)$$

where

$$T=E_0\ (4M_1 M_2)/(M_1+M_2)^2\ \cos^2(\alpha) \quad (5)$$

According to Fig.4, the ion with a mass of M_1 and initial energy E_0 is deflected by the target atom with a mass of M_2. The location of M_2 relative to M_1 is called the impact parameter, which we represent by b. During the collision, M_1 and M_2 deflect with the angles α and β, respectively, relative to the original M_2 pathway. During the collision, the kinetic energy, T, transfers from M_1 to M_2. According to the momentum and energy conversation, this transmitted kinetic energy can be calculated. This kinetic energy T is a function of the angle α, projectile energy, E_0, projectile mass, M_1 and the mass of target atom M_2 in the laboratory system.

The electronic SP in this region is represented by the Bethe-Bloch formula:

$$dE/dx_{ele}=(4\pi Z_1^2 Z_2 e^4)/(m_e v_1^2)\ [\ln((2m_e v_1^2)/I)+\ln(1/(1-\beta^2))-\beta^2-C/Z_2] \quad (6)$$

In Fig.5, we plotted the variations of total mass SP ($S=dE/dx=dE/dx_{nuc}+dE/dx_{el}$) versus proton energy which is calculated by GEANT4/GATE7 simulation with and without NPs injection and compared with Hartree-Fock-Roothaan model without GNPs injection, which is considered below.

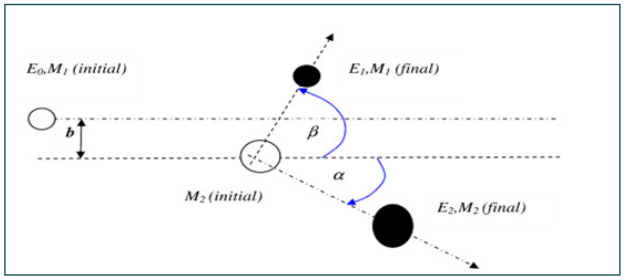

Figure.4. A plan indicating an ion with mass M_1 and initial energy E_0 that collides with an atom with a mass of M_2 and causes it to move with energy E_2 and to reduce its E_1 energy

6-HFR model:

SThe basis of the Hartree-Fock method is the particle time-independent model. The purpose of this model to solving Schrodinger equ. for the motion of electrons at the nuclear potential and the potential arising from all other available electrons. This repetition continues until the density of the resulting electron charge converges with the electron charge density at the start point for one repetition. HFR atomic wave functions are solutions of

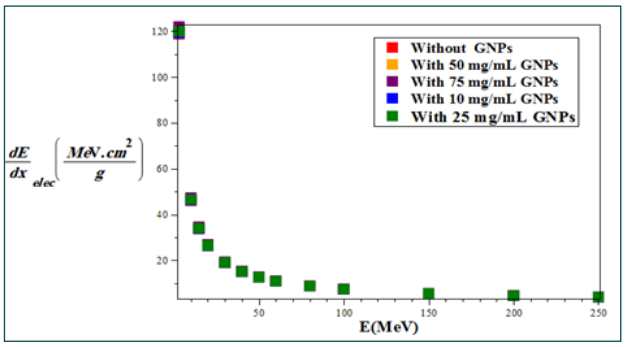

a

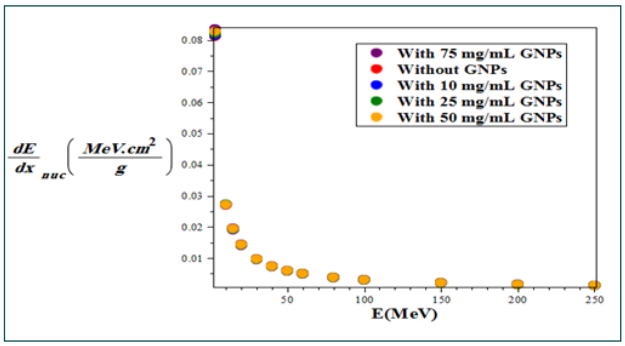

b

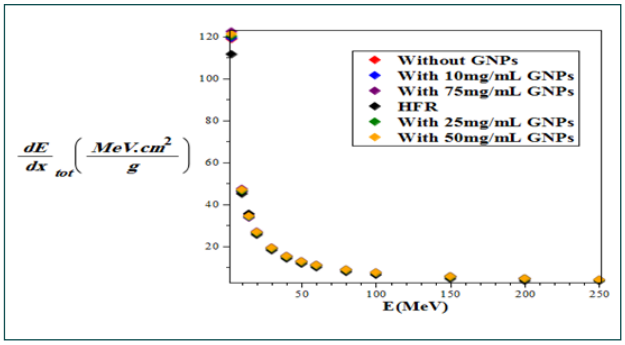

c

Figure.5.view of a) electronic b) nuclear c) total mass SP of proton variations versus proton energy for without and with the injection of GNPs at different selected concentrations in purposed lung phantom and also a comparison with HFR [37] model without injection of GNPs using the GEANT4/GATE7.

Without NPs

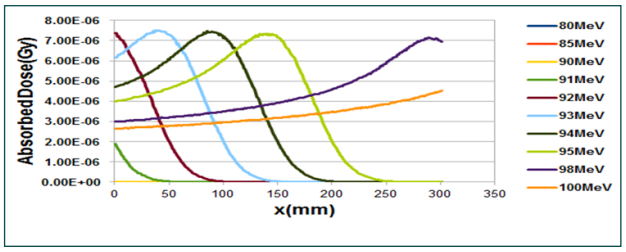

With10mg/ml GNPs

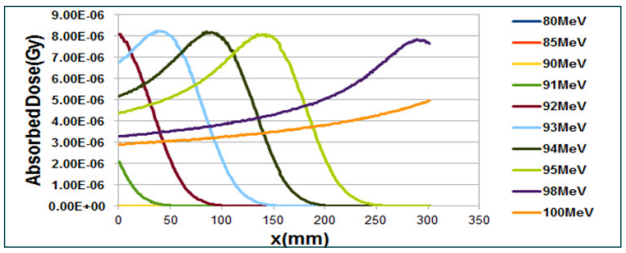

With 25mg/ml GNPs

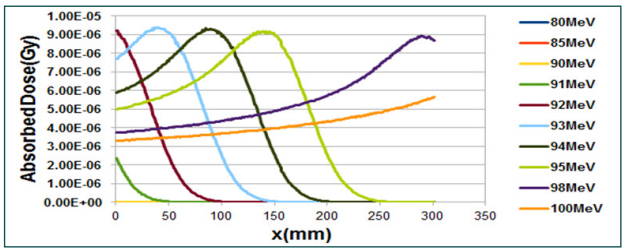

With 50mg/ml GNPs

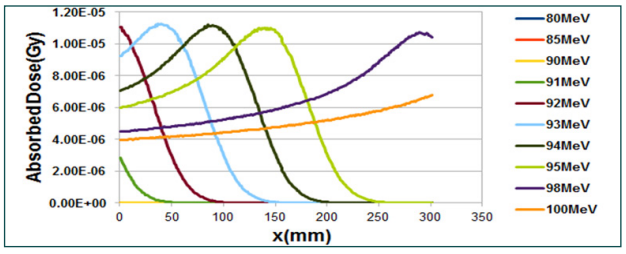

With 75mg/ml GNPs

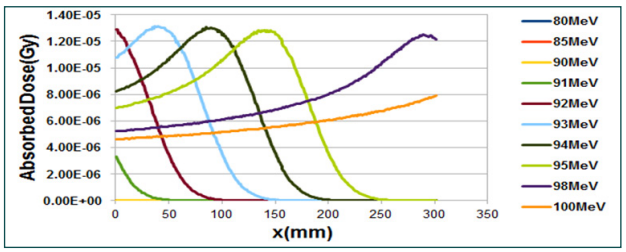

Figure.6. Comparison of the calculated absorbed dose in the lung phantom with or without the injection of GNPs versus depth of penetration for various proton energy (GNPs are considered as a sphere with a diameter of 50 nm and for this calculation, we use GEANT4/GATE7 simulation).

Hartree-Fook's equ. and are shown by Slater–type orbital:

$$w=\sum_i^N d_i \Lambda_i (r) \qquad (7)$$

In this equation d_i is the expansion factor of the orbital.Λ_i (r), is Slater-type orbital and is characterized by the following equation:

$$\Lambda_i (r)=N_i r_i^{n_i-1} e^{(-\alpha i r)} \qquad (8)$$

Here, N_i, n_i , and α_i are constants of normalization, principal quantum number , and orbital exponent value, respectively.

From the observation and comparison of the graphs shown in Fig.5, we found that the minimum SP for all three cases a), b), and c) is related to cases without the injection of GNPs. By increasing the concentration of GNPs, the amount of all types of mass SP gradually and slightly increases. Also, for all modes of without and with the injection of GNPs, with increasing proton energy, all of the SPs are reduced and the minimum SP is related to the nuclear interactions. Electronic mass SP is much higher and has a major share in the total mass SP. Also, the total mass SP without the injection of GNPs using the HFR model is consistent with the GEANT4 simulation model. In Fig.6, the absorbed dose in the proposed lung phantom was compared for two cases: i) with and ii) without the injection of GNPs as a function of penetration depth in the tissue for various proton energy (we note that the selected GNPs are spheres with a diameter of 50 nm). From Figs. 5 and 6, it is seen that with increasing proton energy, mass SP and absorbed dose decrease, but with increasing GNPs concentration, their amount increases. This is due to the production of secondary electrons. It can be seen that from Figs 6a, 6b, 6c and 6d, with increasing energy and distance, from the starting point of the lung phantom, the dose absorbed at the Bragg peaks decreases and the position of the Bragg peak changes with increasing energy. The minimum absorbed dose is related to the case without GNP injection. Our simulations show that by increasing the GNPS injection rate from 10 to 75 mg/ml, the absorbed doses are

increased to 1.1, 1.25, 1.45 and 1.75% for 10, 25, 50 and 75 mg/ml, respectively, compared to the case without GNPs injection. This is because high-Z NPs, such as GNPs, increase the rate of deposited doses inside a tumor or matter due to the increase of secondary electrons and the effect of density. With an assumption that the tumor position is at a depth of 13 cm inside the lung with a width of 2 cm, the optimum energy of Bragg's peak is 93 MeV. Our calculations also show that when protons move with an energy of 250 MeV, the required phantom radius will be more than 30 cm, so that protons with 80≤E(MeV)≤95 can deposit their energy inside the proposed phantom.

7-Bragg-Kleemaan's law:

The Bragg-Kleemaan law for the proton range,R_0, is given in terms of the initial energy E and energy curve dE/dx with the following relation:

$R_0=\alpha E^p$ (9)

$E(x)=\alpha^{-1/p}(R_0-x)^{1/p}$ (10)

$dE/dx=p^{-1}\alpha^{-1/p}(R_0-x)^{(1/p-1)}$ (11)

Where α and p, can be determined from the Bethe equation or from a model that is fitted with the win-energy data, which their values are: α=0.00262. p=1.736. In Fig.7, we plotted 3D variations of proton mass SP and absorbed dose in lung tissue without the injection of GNPs using the Bragg-Kleemaan's law versus proton energy in the energy range 1 ≤E (MeV) ≤250 and in the penetration depth range 1 ≤ x (cm) ≤30.

From the comparison of the graphs for the SP of the Bethe-Bloch (Fig.3-g, using Maple programming) with the model of HFR [37] and our model of the proposed phantom of the lung in this work (Fig.5-c using GEANT4/GATE7 simulation) without the injection of GNPs we found that these models confirm each other well.

8-Physical parameters in proton therapy:

8-1-Multiple-Coulomb Scattering

TA proton passing through matter is likely to be deflected by the nucleus of an atom. This process is known as Coulomb scattering (CS), or more precisely, multiple Coulomb scattering (MCS). Protons and nuclei are positively charged particles, and as a result, are the interaction between them mainly electrostatics. The theory of MCS presents the function of the angular distribution of particles and their specific width. Moliere's theory gives the root mean square of the MCS angles for each energy incidence to the homogeneous plates of any element with very a small thickness. Mean CS angle θ_0 is determined by the Highland relation:

$\theta_0=13.6MeV/pv\ z\sqrt{(L/L_R)}\ [1+0.088\ \log_{10}(L/L_R)\ ]rad$ (12)

Here, p and v are the momentum and velocity of the proton, respectively. z is an atomic number of the projectile. L and L_R are the target thickness and radiation length, respectively, which have the same unit. This formula is valid for a thin slab. L_R is equal to the distance at which

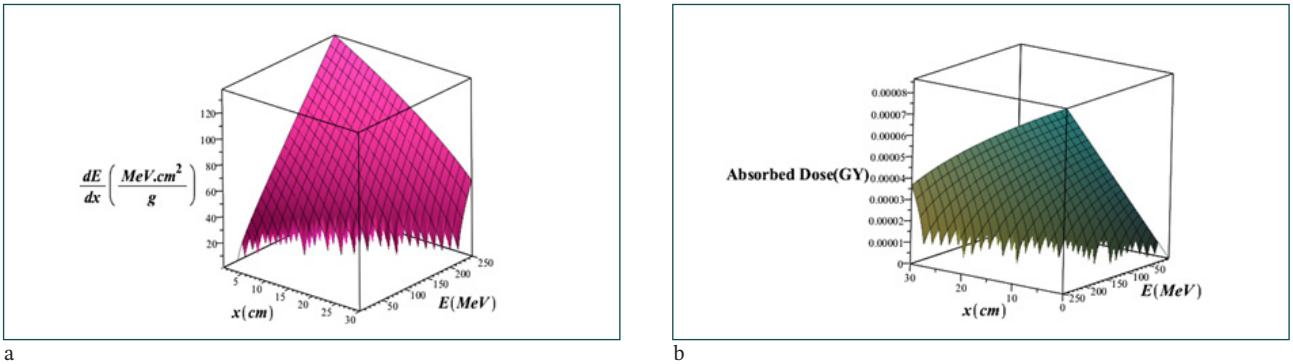

a b

Figure.7.3D view of a) total mass SP and b) absorbed dose in lung tissue without injection of GNPs using Bragg-Kleemaan's law as a function of proton energy in the range 1 ≤E (MeV) ≤250 and penetration depth in the lung tissue in the penetration range 1 ≤ x (cm) ≤30

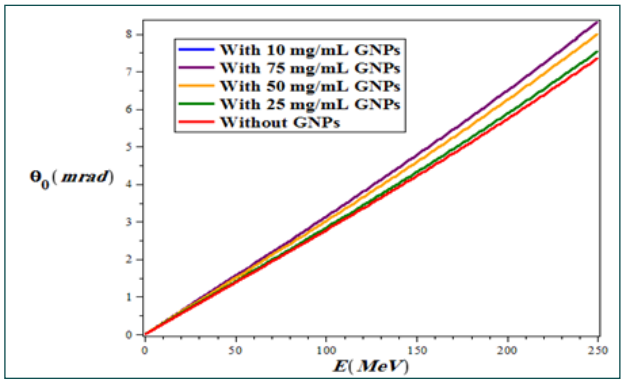

Figure.8. Variations of the mean CS angle versus proton energy in the range of 1 ≤ E (MeV) ≤ 250 with and without the injection of different concentrations of GNPs in the proposed lung phantom.

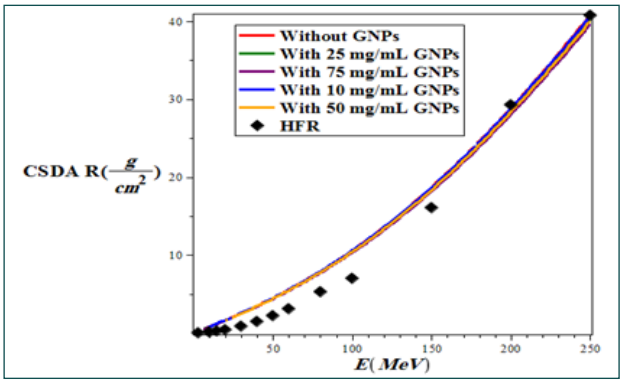

Figure.9. Variations of CSDA proton in lung tissue with and without injection of GNPs using GEANT4/GATE7 simulation versus proton beam energy in the energy range 1≤E (MeV) ≤250 and compare it with HFR model [37].

the energy of the radiation particles decreases by a factor of e^{-1} (≈ 0.37) due to radiation losses. In Fig.8 , we plotted the mean CS angle versus proton energy in the energy range 1 ≤ E (MeV) ≤ 250 with and without the injection of different concentrations of GNPs in the lung phantom.

Seeing Fig.8, we find that, with increasing proton energy, the mean value of the CS angle (θ_0) increases in all conditions, but the lowest θ_0 in the lung tumor is related to the case without injection of GNPs, while with increasing the amount of injection of GNPs into the lung tumor the value of θ_0 gradually increases.

8-2-Proton Range

Here we use the Continuous Slowing Down Approximation (CSDA) method to determine the proton range. CSDA is evaluated by integrating the initial (E_0) and final energy(E_f) of the incident particle onto the target on the inverse of the total SP, which is written by the following [37]:

$$CSDAR=\int_{E0}^{Ef} dE/ S_{tot} \qquad (13)$$

In Fig. 9, we plotted the proton range variations in terms of proton energy in the energy range of 3 ≤ E (MeV) ≤250 without and with the injection of GNPs in the lung tissue, and these diagrams were compared with the results HFR [37] model. As shown in Fig.9, the lowest CSDA range is related to the case without injection GNPs, and with increasing the amount of the concentration of injection GNPs, the CSDA has slightly increased such that at 75 mg/ml of GNPs in the lung tissue the CSDA is maximized and in good compatibility with HFR model.

8-3-Range Straggling

The energy dissipation of an ion in matter is a statistical process and is not a completely definite process, and the Beth equation provides only dissipative energy. This change was first proposed by Bohr, who explained the concept of energy straggling (ES) [39]:

$$d\sigma_E^2(x)/dx \approx 1/(4\pi\epsilon_0^2)\, e^4 \rho_e \qquad (14)$$

Where ρ_e the density of electron is, σ_E is ES and ϵ_0 is the vacuum permittivity coefficient. Equation (14) is true for energy dissipation that is high enough to maintain a Gaussian approximation. However, if the ionic energy remains constant, it is low enough. In 2004 Schulte and his colleagues gave the following differential equation [39]:

$$d\sigma_E^2(x)/dx = K(x) - 2\,(dS(E(x)))/dx\ \sigma_E^2(x) \qquad (15)$$

Where K (x) is as follows:

$$K(x) = z^2 \rho_e\, K(1-1/2\beta^2)/(1-\beta^2) \qquad (16)$$

The range straggling (RS) is defined in terms of energy is given by solving the following equation:

$$d\sigma_R^2/dx = 1/S(E)\ d\sigma_E^2(x)/dx \qquad (17)$$

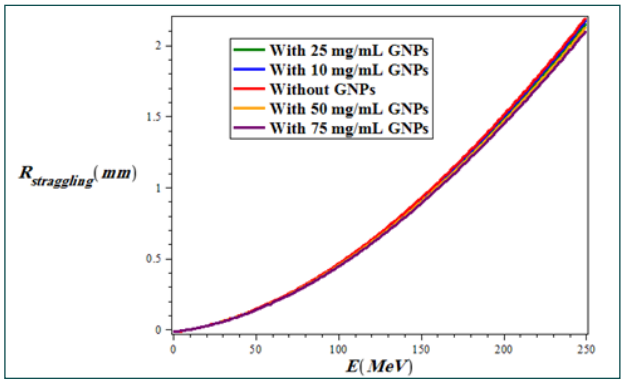

Figure.10. Variations of proton RS in lung tissue for two states i) with and ii) without injection of GNPs using GEANT4 /GATE7 simulation versus proton beam energy in the energy range 1 ≤E (MeV) ≤250.

Where S (E) is total mass SP and σ_R is RS. We calculate the RS as a function of proton energy in the lung tissue for two state: i) without and ii) with the injection of GNPs, and plot it in Fig.10. Seeing Fig. 10, the RS increases with increasing proton energy for both modes of with and without the injection of gold nanoparticles, but the highest RS is for the case of without injection of GNPs and the lowest amount is related to injection of GNPs at a concentration of 75mg/ml. In fact, if the amount of injection of GNPs is more and more, the value of RS decreases.

9-Bortfeld model:

TBortfeld's model is based on the CSDA with additional features that are not considered in the Bethe Bloch model. In many cases, it is better to provide the Bragg curve instead of using numerical or measured data. 1997, Brownfield paper presents a rough analysis of the Bragg curve. The accuracy of this model is in the proton energy range of 10 to 250 MeV. Four basic principles of this model are: i) a power-law equation that represents the energy-range dependence, ii) a linear model for reducing flounce arising from nuclear interactions, iii) assuming a fraction of localized released energy, iv) a Gaussian approximation of the distribution of the RS and presentation energy spectrum for multi-energy beams in the form of Gaussian distribution with a linear tail [40]. From this theoretical model two types of deep doses are achievable: a) deep dose formula without examining the effects of proton straggling range is [40]:

$$D(z)=(\varphi_0(R_0-z)^{(1/p-1)}+\beta(1+p\gamma)(R0-z)^{1/p})/\rho(1+\beta R_0 \quad)p\alpha^{1/p} \quad (18)$$

Note that the above equation is valid for $z<R_0$. For $z>R_0$, $D(z)=0$. The above equation can be rewritten as follows:

$$D(z)=D_a(z)+D_b(z)=a_a(R_0-z)^{(1/p-1)}+a_b(R_0-z)^{1/p} \quad (19)$$

The first term $D_a(z)$ is the contribution of dose due to proton without nuclear interactions. The second term, $D_b(z)$, represents the dose transmitted by a relatively small fraction of protons having nuclear interactions. b) Deep dose with the SR of the proton's effects is [40]:

$$D(z)=\varphi_0 e^{-\zeta 2/4} \sigma^{1/p} \Gamma(1/p)/(\sqrt{2\pi}\rho(1+\beta R_0)p\alpha^{1/p}[1/\sigma D(p)_{-1/p}(-\zeta)+\beta(1/p+\gamma)D(p)_{-1/p-1}(-\zeta)] \quad (20)$$

Some of the "special functions" and the parameters that appear in equations (18) to (20) are defined as follows: Geiger's law is: $R_0=\alpha E_0^p$, the range R_0 is determined by the exponent dependence on energy E_0, where p and α are constant. In ICRU 49, p = 1.77, but the Bragg-Kleeman law describes the constant α. According to Geiger's law, the proton traverses the maximum range of R_0 in initial energy E_0. Therefore, in the energy E(x) along x (direction of motion), the proton travels the distance R_0-x, which is the same as the solutions of Weber's differential equation. Γ(z) is the gamma function which is defined by Euler's formula. The functional relationship between σ and R_0 can be given with the following approximation:

$$\sigma 2\approx(\alpha' p^3\alpha^{2/p}/(3p-2))R_0^{(3-2/p)} \quad (21)$$

Where α' is a factor which depends on the stopping matter through α. R_0 and σ are in cm. In the Borteff model, γ is the energy fraction that is locally absorbed. In this model, γ=0.6 and $\beta\approx0.012cm^{-1}$. φ_0 is the particle flounce which is the number of particles per cm^2. Suppose$\zeta=(R0-x)/\sigma$.In Fig. 12, 3D variations of absorbed dose with the effects of the proton straggling versus pen-

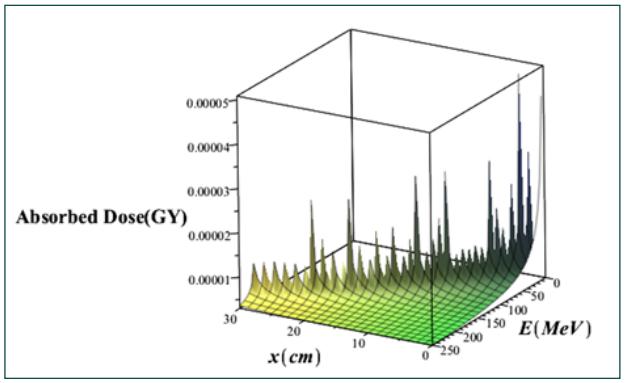

Figure.11. 3D variations of deep dose without considering the effects of proton SR versus penetration depth and proton beam energy

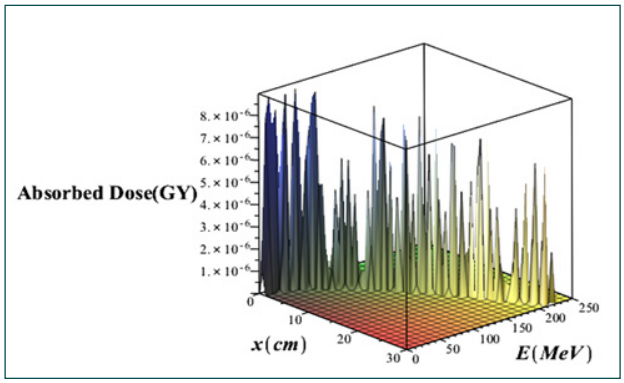

Figure.12. 3D variations of absorbed dose considering effects of proton straggling range versus the penetration depth and energy of the proton beam without injection of gold nanoparticles

etration depth and proton beam energy in the lung tissue without the injection of GNPs have been brought. Comparison of Figs.11 and 12 it is seen that in the case without injection of GNPs, the absorbed dose value taking into account the effects of the RS, is less than the amount of absorbed dose regardless of the absorption effects

10-Conclusion:

In summary, in this paper, the absorbed dose is estimated for the proposed lung phantom in the five cases: i) using theoretical quantum relativistic Bethe-Bloch model without GNPs using Maple programming (Fig.3), ii) using GEANT4/GATE7 simulation through the proposed phantom(Fig.6), iii) using Bragg-Kleemaan law using Maple programming (Fig.7b), iv/v) using the Bertfeld model, without/with considering effects of proton RS using Maple programming (Fig.11/Fig.12). Comparing the results of the above cases, we find that Bragg's peak is only seen in the Bethe-Bloch model and GEANT4/GATE7 simulation model of the proposed phantom, and the values of absorbed dose from each purposed model are different, but this difference is not so much, and the proposed GEANT4/GATE7 simulation model is more accurate than the other models, also the results of this proposed model confirm that injection of GNPs into the lung tumor increases the absorbed dose and the enhancement of concentration of the GNPs increases the absorbed dose values. Finally, it should be noted that since in proton RT, proton beams are sensitive to various types of uncertainty, such as respiratory movement, change in patient location, and tumor contraction, more research is needed to optimize proton radiotherapy for lung cancer. This requires a greater understanding of physics to create designs that are faced with uncertainties.

REFERENCES

1. Palma D.A. Senan S., Oberije C., Belderbos J., de Dios N.R., Bradley J.D., Barriger R.B., Moreno-Jimenez M., Kim T.H., Ramella S., et al. Predicting esophagitis after chemoRT for non-small cell lung cancer: An individual patient data meta-analysis. Int. J. Radiat. Oncol. Biol. Phys, 87,690–696, 2013.
2. Wolf J, Patno ME, Roswit B, D'Esopo N. Controlled study of survival of patients with clinically inoperable lung cancer treated with RT. Am J Med, 40, 360-367, 1966.
3. Hainfeld JF, Dilmanian FA, Slatkin DN, Smilowitz HM. Radiotherapy enhancement with gold nanoparticles. J Pharm Pharmacol, 60,8, 977-85,2008.
4. Maggiorella L, Barouch G, Devaux C, et al. Nanoscale radiotherapy with hafnium oxide nanoparticles. Futur Oncol.,81,8,1167-1172,2012.
5. Sancey L, Lux F, Kotb S, et al. The use of theranostic gadolinium-based nanoprobes to improve radiotherapy efficacy. Br J Radiol. 87,20140134, 2014.
6. Kim J-K, Seo S-J, Kim K-RK-H, et al. Therapeutic application of metallic nanoparticles combined with particle-induced X-ray emission effect. Nanotechnology, 21,425102, 2010.

7. Polf JC, Bronk LF, Driessen WHP, et al. Enhanced relative biological effectiveness of proton radiotherapy in tumor cells with internalized gold nanoparticles. Appl Phys Lett. 98:193702, 2011.
8. Schlathölter T, Lacombe S, Eustache P, et al. Improving proton therapy by metal-containing nanoparticles: nanoscale insights. Int J Nanomed, 11,1549, 2016.
9. Butterworth K T, Wyer J A, Brennan-Fournet M, Latimer C J, Shah M B, Currell F J and Hirst D G. Variation of strand break yield for plasmid DNA irradiated with high-Z metal nanoparticles. Radiat. Res. 170 381–7, 2008.
10. Porcel E, Liehn S, Remita H, et al. Platinum nanoparticles: a promising material for future cancer therapy? Nanotechnology, 21:85103, 2010.
11. Jain S, Coulter JA, Butterworth KT, et al. Gold nanoparticle cellular uptake, toxicity and radiosensitisation in hypoxic conditions. Radiother Oncol, 110:342–7, 2014.
12. Lewis H. W., Phys. Rev. 78 526, 1950.
13. ICRU Stopping powers and ranges for protons and α-particles ICRU Report 49 (Bethesda, MD), 1993.
14. Reynaert N, Vandermarck S, Schaart D, Vanderzee W, Vanvlietvroegindeweij C, Tomsej M, Jansen J, Heijmen B, Coghe M, and Dewagter C.Monte carlo treatment planning for photon and electron beams. Radiat. Phys. Chem. 76, 643–686 ,2007.
15. Murphy M. J, Balter J. M, Balter S, BenComo J. A, Das I. J, Jiang S. B, Ma C. M, Olivera G. H, Rodebaugh R. F, Ruchala K. J, Shirato H, and Yin F. F.The management of imaging dose during image-guided radiotherapy: Report of the AAPM Task Group 75. Med. Phys. 34, 4041– 4063, 2007.
16. Ljungberg M and Strand S. E.A Monte Carlo program for the simulation of scintillation camera characteristics. Comput Methods Programs Biomed 29, 257–272 ,1989.
17. Harrison R and Vannoy S.Preliminary experience with the photon history generator module of a public-domain simulation system for emission tomography. in Proceedings of the IEEE Nuclear Science Symposium and Medical Imaging Conference, 1154–1158, 1993.
18. Cañadas M, Arce P, and Rato Mendes P.Validation of a small-animal pet simulation using gamos: A GEANT4-based framework. Phys. Med. Biol. 56, 273–288, 2011.
19. LANL, MCNPX 2.6.0 Users's Guide, Technical Report No. LA-CP-07 1473, 2008.
20. Battistoni G, Muraro S, Sala P, Cerutti F, Ferrari A, Roesler S, Fasso A, and Ranft J.The FLUKA code: Description and benchmarking. in Hadronic Shower Simulations Workshop, edited by M. Albrow and R. Raja (AIP Conference, Fermilab, Batavia, IL), Vol. 896, 31–49, 2006.
21. Ferrari A, Sala P, Fasso A, and Ranft J. FLUKA: A Multi-Particle Transport Code. Technical Report No. INFN/TC 05/11, SLAC-R-773, CERN2005-10, 2005.
22. Perl J, Shin J, Faddegon B, and Paganetti H.TOPAS : An innovative proton Monte Carlo platform for research.Med. Phys. 39, 6818–6837 ,2012.
23. Walters B. R. B, Kawrakow I, and Rogers D. W. O.History by history statistical estimators in the beam code system. Med. Phys. 29, 2745–2752 ,2002.
24. Kawrakow I and Fippel M.Investigation of variance reduction techniques for Monte Carlo photon dose calculation using XVMC. Phys. Med. Biol. 45, 2163–2183 ,2000.
25. Jan S, Santin G, Strul D, Staelens S, Assié K, et al.Gate: A simulation toolkit for PET and SPECT. Phys. Med. Biol. 49, 4543–4561 ,2004.
26. Jan S, Benoit D, Becheva E, Carlier T, Cassol F, et al .GATE V6: A major enhancement of the gate simulation platform enabling modelling of CT and radiotherapy. Phys. Med. Biol. 56, 881–901 ,2011.
27. The OpenGate Collaboration, http://www.opengatecollaboration.org, 2014.
28. The OpenGate Collaboration, http://git.opengatecollaboration.org/git/ opengate-public.git, 2014.
29. Paganetti H.Dose to water versus dose to medium in proton beam therapy. Phys. Med. Biol. 54, 4399–4421 ,2009.
30. Grevillot L, Bertrand D, Dessy F, Freud N, and Sarrut

D.Gate as a GEANT4-based Monte Carlo platform for the evaluation of proton pencil beam scanning treatment plans. Phys. Med. Biol. 57, 4223–4244 ,2012.
31. Tedgren Å. C and Carlsson G. A.Specification of absorbed dose to water using model-based dose calculation algorithms for treatment planning in brachytherapy. Phys. Med. Biol. 58, 2561–2579 ,2013.
32. Jiang H, Seco J, and Paganetti H.Effects of Hounsfield number conversion on CT based proton Monte Carlo dose calculations. Med. Phys. 34, 1439–1449 ,2007.
33. Jiang H and Paganetti H.Adaptation of GEANT4 to Monte Carlo dose calculations based on CT data. Med. Phys. 31, 2811–2818 ,2004.
34. Sarrut D and Guigues L.Region-oriented CT image representation for reducing computing time of Monte Carlo simulations. Med. Phys. 35, 1452–1463 ,2008.
35. Wayne D Newhauser and Rui Zhang. The physics of proton therapy. Phys. Med. Biol. 60 R155–R209, 2015.
36. Jens Lindhard and Allan H. Sorensen, PHYSICAL REVIEW A, 53, 4, 2443-2456, 1995.
37. Metin Usta I. Mustafa Çağatay T. Stopping power and range calculations in human tissues by using the Hartree-Fock-Roothaan wave functions. Radiation Physics and Chemistry · March 2017.
38. Highland VL. Some practical remarks on multiple scattering. Nucl Instrum Methods, 129,497–9. 1975.
39. Ulmer W and Schaner B. Foundation of an analytical proton beamlet model for inclusion in a general proton dose calculation system. Radiation Physics and Chemistry, vol. 80, 2011.
40. Bortfeld T. An analytical approximation of the Bragg curve for therapeutic proton beams. Med Phys. 24,12,2024-33, 1997.